IMPURITY DECORATION OF NATIVE VACANCIES IN Ga AND N SUBLATTICES OF GALLIUM NITRIDE

Sami Hautakangas

Laboratory of Physics
Helsinki University of Technology
Espoo, Finland

Abstract

The effects of impurity atoms as well as various growth methods to the formation of vacancy type defects in gallium nitride (GaN) have been studied by positron annihilation spectroscopy. It is shown that vacancy defects are formed in Ga or N sublattices depending on the doping of the material. Vacancies are decorated with impurity atoms leading to the compensation of the free carriers of the samples. In addition, the vacancy clusters are found to be present in significant concentrations in n-type as well as in p-type GaN.

Nitrogen vacancies compensate Mg impurities in magnesium doped GaN. The high Mg content creates a defect profile with a low vacancy concentration near the surface. Post-growth annealing dissociates V_N-related complexes activating the p-type conductivity. Also the vacancy profile is made homogeneous by thermal treatment in highly Mg-doped GaN.

The direct experimental evidence of oxygen decorated Ga vacancy is obtained in O-doped n-type GaN. The present study shows that V_{Ga}-O_N is distinguishable from an isolated Ga vacancy by positron annihilation spectroscopy. Yellow luminescence (YL) is common in n-type GaN, which is usually related to Ga vacancy defects. However, carbon doped semi-insulating GaN is exhibiting strong YL emission, but without the presence of Ga vacancies. The YL is attributed to C interstitials. The investigations concerning silicon doped GaN and GaN grown by the mass-transport method reveal vacancy type defects, which were identified as vacancy clusters.

Preface

This thesis has been prepared at the Laboratory of Physics, Helsinki University of Technology during the years 2002-2005. I want to express my gratitude to my supervisor Prof. K. Saarinen. He has made possible not only the fast accomplishment of this thesis but also the publishing of these results in recognized publication series. With the help of Kimmo's excellent guidance and superior wisdom I have been able to overcome the encountered drastic problems. He has always been willing to deliver his knowledge whether I have needed a small assistance in paper work or been desperate for help with data analysis.

I want to thank Prof. P. Hautojärvi for the administrative role during this project. He has given me a great support in finding motivation and confidence in the field of physical science. Prof. M. Puska and his group has given me very valuable information about the computational aspects of theoretical modeling. Very talented positron group, i.e. individuals at the basement, deserves thanks for enthusiastic work-related and non-work-related conversations. The construction group including D.Sc. K. Rytsölä has always given me help to fix the problems with positron beams.

My mother and father has supported me greatly in every single moment during finishing up my studies. They have given me the idea of hard work, and how it can sometimes lead to success. A. Alho has given me a helping hand when ever the childcare was needed. Nuuti and Hilla are the innermost reasons to get up (early!) in the morning and face the facts of the surrounding environment. And there is no man without a great woman besides him. Susanna has, among other things, offered me an excellent opportunity to practice my skills in scientific or in unscientific debates.

Hyvinkää, April 29, 2005

Sami Hautakangas

Contents

List of publications

This thesis consists of an overview and the following publications:

I S. Hautakangas, J. Oila, M. Alatalo, K. Saarinen, L. Liszkay, D. Seghier, and H. P. Gislason, *Vacancy defects as compensating centers in Mg-doped GaN*, Physical Review Letters **90**, 137402 (2003).

II S. Hautakangas, K. Saarinen, L. Liszkay, and J. Freitas, *The role of open volume defects in Mg-doped GaN studied by positron annihilation spectroscopy*, submitted for publication in Physical Review B.

III P. Laukkanen, S. Lehkonen, P. Uusimaa, M. Pessa, J. Oila, S. Hautakangas, K. Saarinen, J. Likonen, and J. Keränen, *Structural, electrical, and optical properties of defects in Si-doped GaN grown by molecular-beam epitaxy on hydride vapor phase epitaxy GaN on sapphire*, Journal of Applied Physics **92**, 786 (2002).

IV R. Armitage, W. Hong, Q. Yang, H. Feick, J. Gebauer, E. R. Weber, S. Hautakangas, and K. Saarinen, *Contributions from gallium vacancies and carbon-related defects to the "yellow luminescence" in GaN*, Applied Physics Letters **82**, 3457 (2003).

V S. Hautakangas, V. Ranki, I. Makkonen, M. J. Puska, K. Saarinen, X. Xu, and D. C. Look *Direct experimental evidence of impurity decoration of Ga vacancies in GaN*, submitted for publication in Physical Review Letters.

VI T. Paskova, P. P. Paskov, E. M. Goldys, E. Valcheva, V. Darakchieva, U. Södervall, M. Godlewski, M. Zielinski, S. Hautakangas, K. Saarinen, C. F. Carlström Q. Wahab, and B. Monemar, *Characterization of mass-transport grown GaN by hydride vapour-phase epitaxy*, Journal of Crystal Growth **273**, 118 (2004)

The author has had an active role in all stages of the work reported in this thesis. He has been involved in planning and performing of the positron experiments excluding the slow positron lifetime measurements and sample preparation. The analysis of all experimental positron data has been made by the author. He has written Publications I, II and V and has had the main responsibility of the sections concerning the positron annihilation experiments in Publ. IV and VI. The theoretical studies concerning the atomic superposition method have been performed by the author.

Chapter 1

Introduction

The requirement for more efficient optical and electronic components has created a big variety of new semiconductor materials. Especially, gallium nitride (GaN) is an object of a particular interest because it can be used in optoelectronic components, like blue light emitting diodes and lasers due to its large forbidden band gap. By special treatments, i.e. adding impurity atoms, heat treatment or irradiation, the desired properties of GaN can be reached. Although the blue light emitting devices based on GaN are available in markets, the details of the emission are still under some debate.

Doping of semiconductor material is the most efficient way to increase the free carrier concentration by producing an energy level in a forbidden energy gap. The native defects, like vacancies and lattice atoms at interstitial sites, also have an effect on the material properties. Native defects could be controlled for example by carefully adjusting the growth conditions, but they are in practice difficult to avoid. In addition the unintentional or intentional dopings affects to the formation of native defects. Hence, the detailed knowledge of doping and its influence to the material properties are essential aspects to improve the performance of optical and electronic components.

We have studied vacancy type defects with positron annihilation spectroscopy. Because of their positive charge, positrons probe negative and neutral defects of the material, especially vacancies. The information about vacancies is achieved in two ways: as a narrowing of the positron-electron annihilation energy spectrum and as an increase of the positron lifetime. In addition, the annihilation data give information about the chemical environment of the vacancy and enable quantitative analysis of vacancy concentrations.

In Publ. I and II we have shown the positron trapping at vacancies in N sublattice in GaN. The positron annihilation data show that the nitrogen vacancy (V_N) is

complexed with a magnesium impurity producing a neutral defect. Vacancy type defects are shown to form during the growth and their concentrations can be controlled by the Mg impurity concentration. The monovacancy type defects in Mg doped GaN are formed when the doping exceeds 10^{18} cm^{-3}. When the doping is increased close to the solubility limit of Mg in GaN the vacancy cluster type defects are formed. The high Mg doping level generates also a defect profile where the lower concentration of vacancies is located near the sample surface.

The investigations concerning silicon doped GaN reveal vacancy cluster type defects (Publ. III). The molecular beam epitaxy (MBE) growth of GaN introduces also a significant amount of Ga vacancy-donor complexes. The concentration of vacancy clusters decreases as Si concentration is increased.

The Ga vacancy formation in semi-insulating GaN doped with carbon is studied in Publ. IV. The yellow luminescence (YL) of n-type GaN is usually related to Ga vacancies. However, moderate C doping increases YL but almost no Ga vacancies are detected in semi-insulating (SI) GaN:C samples [IV]. The defect behind YL in SI GaN:C seems to be different from the one in low carbon doped n-type GaN. When the interstitial carbon concentration is comparable to or exceeds the Ga vacancy concentration the YL mechanism is proposed to change.

Oxygen impurities promote the creation of Ga vacancies because the O atoms increase the n-type conductivity which lowers the formation energy of V_{Ga}. In Publ. V the positron measurement shows that isolated V_{Ga} is distinguishable from V_{Ga}-O_N. Although the electron configuration of N and O atoms is almost the same a clear difference in the positron data is seen. The O atom has electrons with higher momenta which is seen as a higher intensity in the high momentum region of the annihilation distribution.

Because of the extreme conditions needed for the growth of bulk GaN the epitaxial methods have proved to be a more convenient way to produce GaN layers. However, the epitaxy introduces significant amount of dislocations because of the lattice mismatch between GaN and substrate material. To reduce the density of dislocations many lateral overgrowth methods have been introduced. In Publ. VI we have investigated the vacancy type defects of mass-transport (MT) grown GaN. The high impurity concentrations in the MT growth area are accompanied by the formation of vacancy clusters. This is related to different growth velocities between the normal and MT grown area as well as the high unintentional impurity concentration of the MT region.

Chapter 2

Experimental methods

The scope of this work has been to investigate the defects in semiconductor materials by positron annihilation spectroscopy. As positive particles positrons are able to sense the neutral and negative charged defects, especially vacancies. A vacancy is an empty lattice site. In a perfect lattice atoms have well-defined sites and the background potential arising from ion cores is periodic. However, many types of defects are formed during growth or by post-growth treatments, causing perturbations to this background potential. Locally reduced positive background leads to trapping of positrons. The information about the micro-structure of the material is obtained from the annihilation radiation of positron-electron pairs.

The most-used laboratory source of positrons is ^{22}Na because it is easily available and the positron yield is high (90.4 %). The energy distribution of the positrons is continuous up to an energy of 540 keV and thus the positrons can penetrate deep into the sample. The additional advantage of this isotope is the production of 1.27 MeV γ-quantum almost simultaneously with the positron which enables the implementation of positron lifetime measurements.

After implantation into the material positrons slow down i.e. thermalize with the surroundings. This takes usually 1-10 ps, which is a short time when compared to the positron lifetime in a lattice. Few annihilations thus occur during the slowing down. During diffusion positrons can get trapped by negative or neutral defects. Finally they annihilate with an electron into two 511 keV γ-quanta. By measuring the time interval between the birth-γ and the annihilation γ one can determine the lifetime of the positron in the material.

In a vacancy the electron density is decreased because of the missing ion core. This is seen as an increased positron lifetime. Positron lifetime measurements are used to identify different vacancy type defects and to determine their concentrations. Because of the high energy of the positrons from a ^{22}Na source they can

be used to probe the properties of bulk samples, which are a couple of hundreds of micrometers thick. The thickness of the samples prevents positrons from penetrating outside the material and makes sure the annihilation events occur in the sample.

In order to study thin epitaxial layers and to determine the defect profiles a mono-energetic positron beam is needed. The slowing down of the positrons from their initial energies is done with thin tungsten moderators, which have a negative work function for positrons. Positrons from the source penetrate to the W foil, thermalize and some of them are able to diffuse to the surface before annihilation. From the surface they are pushed to the vacuum with an energy of the work function. The efficiency of the W foils is usually $\sim 10^{-4}$, which reduces significantly the intensity of the slow positron beams. In addition, during the moderation the information of the birth-γ is lost, which makes it more difficult to implement the positron lifetime measurement. Despite the difficulties, positron lifetime beams have been successfully constructed [1,2]. In the lifetime experiments of this work, the pulsed positron beam of the Universität der Bundeswehr in Munich was applied.

Slow positrons can be more easily used for Doppler measurements, where the energy distribution of the annihilation-quanta is recorded. The broadening of the annihilation energy line is arising from the momentum of electrons. The positron is thermalized, i.e. its energy is ~ 26 meV at room temperature, which is much smaller than the average kinetic energy of an electron in material. Hence, the recorded Doppler broadening of the annihilation line yields information on the momentum distribution of electrons.

Electron wave functions from neighboring atoms extend to the vacancy reducing the electron average momentum, which is seen as a narrowing of the energy distribution of the annihilation photons. By comparing the annihilation lines between samples one can characterize the defects. Doppler broadening spectroscopy is used to identify the vacancy and it is also a powerful tool to determine the chemical environment of the annihilation site. By combining positron lifetime and Doppler measurements very reliable information about the vacancy type defects is obtained.

The Doppler broadening of the 511 keV annihilation line is measured by a high-resolution Ge detector. The broadening is characterized by line shape parameters, low momentum parameter S and high momentum parameter W. The S parameter measures the fraction of counts in the central part of the peak ($\pm$ 0.95 keV around the center) and the W parameter measures the fraction of counts in the wing areas. The S parameter hence describes the annihilation with low momentum valence electrons while the W parameter describes the annihilations with high momentum core electrons. The annihilation at a vacancy increases the S parameter and

decreases the W parameter because of the narrowed momentum distribution. The ideal positron lifetime spectrum is of the form

$$-\frac{dn(t)}{dt} = \sum_i I_i \lambda_i exp[-\lambda_i t],$$ (2.1)

where $n(t)$ is the number of positrons alive at time t, $\lambda_i = 1/\tau_i$ is the decay constant of an individual positron state i and I_i is the state intensity. The sum of the relative intensities is $\sum_i I_i$=1. The decomposition of the measured spectrum gives the lifetimes of individual positron states. In practice the number of lifetime components is limited to three because of the finite statistics. The center of mass, however, is always a reliable parameter, and it coincides with an average lifetime $\tau_{ave} = \sum_i I_i \tau_i$. The presence of vacancy type defects is easily measured as a long average lifetime compared to the bulk lifetime obtained in defect-free lattice.

In practice the measured lifetime spectrum is always a convolution between an ideal spectrum and the time resolution function of the spectrometer. This is also the case in the Doppler measurements where the broadening effect is typically twice as large as the energy resolution. Often the relative changes of the annihilation distribution are most important and the deconvolution is not necessary. However, when one makes comparisons, for example, with theoretically obtained results the resolution of the detectors has to be taken into account.

The annihilation parameters recorded in a particular sample are superpositions of parameters characterizing the annihilations at different positron states weighted with corresponding annihilation fractions η

$$A = \eta_b A_b + \sum_i \eta_i A_i,$$ (2.2)

where A is the measured τ_{ave}, S or W and A_i the annihilation parameter of individual positron state i. Letter b denotes the annihilation parameters of the delocalized positrons. If only one vacancy type defect is trapping positrons the measured annihilation parameters hit the line connecting points (A_b, A_b) and (A_V, A_V) in the (S,W), (S,τ_{ave}) or (W,τ_{ave}) plane.

In addition to vacancies also negative ions are sensed by positrons as attractive centers. The electron density around an ion is almost the same as in bulk, leading to the same annihilation characteristics. Ions are typically observed as defects competing with vacancies as positron traps. The binding energy of a positron at a negative ion is usually 10-100 meV. By elevating the measuring temperature positrons can escape from these shallow traps. The detrapped positron can be further trapped by vacancy type defects. In practice negative ions decrease the average lifetime and S parameter when the measuring temperature is decreased.

Chapter 3

Vacancy type defects in magnesium doped GaN

There are three limiting factors when determining the doping efficiencies of semiconductors to obtain the desired optical and electrical properties: i) solubility of dopant atoms, ii) ionization energy and iii) compensation. The solubility corresponds to the maximum concentration of doping atoms which can be attained in a semiconductor material under thermodynamical equilibrium. This concentration depends on temperature and growth environment. With very high doping levels it may become favorable for the impurity atom to form a different phase, and this limits the doping concentration.

Ionization energy determines the fraction of free carriers emitted from the dopant impurities at given temperature. A high ionization energy can limit a free carrier concentration so that only 1 % or less of the doping atoms are emitting carriers to the conduction or valence bands. This leads to quenching of the free carrier concentration. Ionization energy depends not only on the properties of the impurity atom but also on the intrinsic properties of the material such as the effective mass and the dielectric constants. For classical shallow dopants the ionization energies are very similar independently of the chemical identity of the impurity.

In practice unintentional impurities play an important role. In many growth methods the lattice and doping atoms are incorporated into the material together with impurities, which can act as compensating centers to the doping atoms. While the compensation by impurity atoms may be controlled in a clean growth environment, native defects can sometimes form a severe problem, which cannot be overcome by an ultimate growth control.

It has been shown by theoretical calculations that vacancy type defects are the most important native point defects in gallium nitride (GaN). The nitrogen va-

cancy (V_N) has the lowest formation energy regardless of the growth conditions in p-type and insulating GaN [3]. The gallium vacancy (V_{Ga}), on the other hand, is prominent in n-type GaN. These defects are compensating centers for p-type and n-type GaN, respectively. The dominant role of native vacancy formation can be attributed to the relative differences in Ga and N atom sizes: interstitial and anti-site defects have much higher formation energies than vacancies.

While n-type conductivity of GaN is easily achieved with Si or O doping, the p-type material is generally much more difficult to fabricate. Mg doped GaN grown by metal organic chemical vapor deposition (MOCVD) is semi-insulating after the growth and has to be annealed at moderate temperature in order to achieve significant hole concentrations [4]. This behavior is generally attributed to hydrogen atoms [5,6] that bond to the Mg acceptors passivating them electrically. The heat treatment (typically at 500 - 800 °C) dissociates the Mg-H complexes leading to the p-type conductivity due to the hole emission from isolated Mg atoms. In the next section the competitive roles of N vacancies and the vacancy clusters to the compensation of Mg doped GaN are discussed in more detail.

3.1 Nitrogen vacancies as compensating centers

In Publ. I we have studied three Mg-doped GaN layers with a thickness of 2μm grown on a sapphire substrate by metal-organic chemical vapor deposition (MOCVD) at EMCORE ltd. The as-grown sample was electrically resistive and the other two samples were annealed under N_2-flow. The second sample was annealed at 500 °C for 5 minutes, and had a net space charge concentration N_a-N_d=3 × 10^{16} cm^{-3} as determined by capacitance-voltage measurements. This concentration is generally equal to the net hole concentration p in the valence band. The third sample was annealed at 800 °C for 30 minutes and had N_a-N_d=1 × 10^{17} cm^{-3}. The electrical experiments as well as the thermal treatments were done at the University of Iceland, Reykjavik. A Mg-doped sample ($p \sim 10^{18}$ cm^{-3}) grown by molecular-beam epitaxy (MBE) at 800 °C was measured as a reference.

In the high temperature region (T > 400 K) the valence annihilation parameters have a clear order depending on the annealing temperature (Fig. 3.1). The sample annealed at 800 °C has almost the same S-parameter level as that in the bulk GaN lattice and the S parameter in other samples is much higher. The average momentum of electrons at vacancies is less than in the bulk lattice, which leads to a narrower positron-electron momentum distribution and increased S parameter. The results in Fig. 3.1 are thus a clear indication of vacancies in the as-grown sample. Furthermore, the decrease of the S parameter shows that the vacancy concentration decreases in the annealings at 500 - 800 °C.
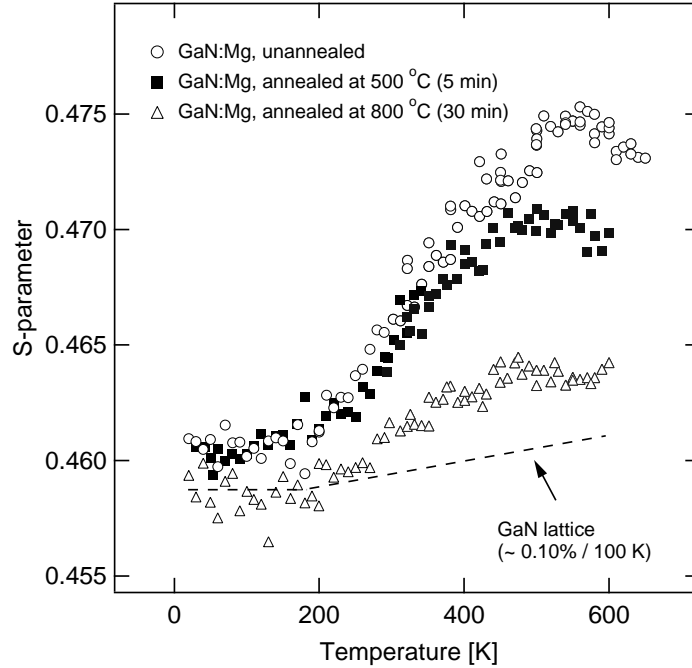
Figure 3.1: The valence annihilation parameter S as a function of measuring temperature.

In Fig. 3.1 the S parameter decreases toward the GaN bulk value in the low temperature region. This behavior is typically observed when positron trapping at vacancies is prevented by other defects, which do not have open volume [7]. As shown before, both negative Mg ions [8] and dislocations [9] trap positrons in GaN at low temperatures. Above 400 K the S parameter saturates, indicating that positrons have enough thermal energy to totally escape from these shallow traps. We concentrate here on the data recorded at this temperature region, because it is dominated by a clean signal of positron annihilation at vacancy defects. Notice that the presence of vacancy defects has been shown to be independent of the dislocation density in n-type GaN, suggesting that the open volume defects are rather in the grain interior than at the grain boundary [9].

In the positron lifetime experiments performed with the pulsed positron beam, we used a p-type Mg doped GaN layer grown by molecular beam epitaxy (MBE) as a reference (Fig. 3.2). The lifetime spectrum of this sample shows a single exponential component of 154 ps. Within experimental accuracy, this is the same value as reported in conventional lifetime experiments in thick bulk crystals [10]. This implies that positrons in the MBE grown GaN:Mg crystals annihilate in the lattice and no vacancies are observed.
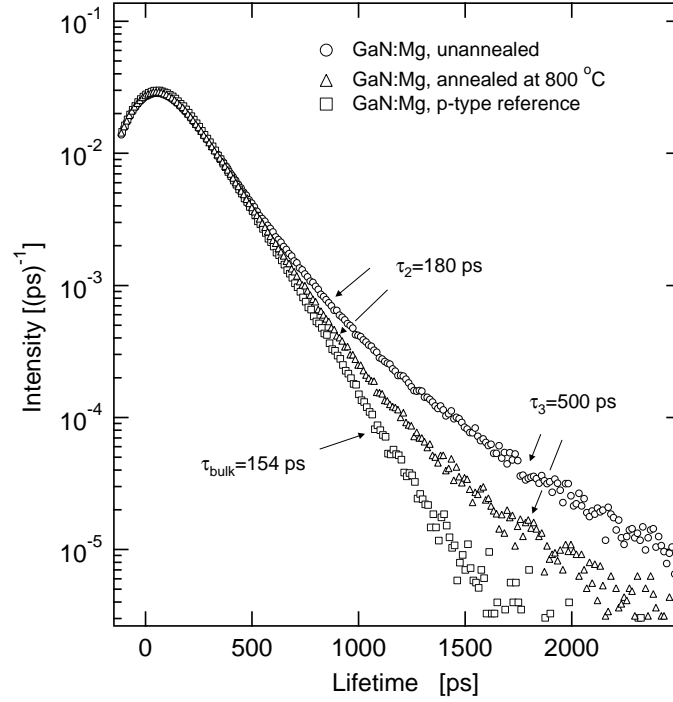
Figure 3.2: The measured positron lifetime spectra from MOCVD grown GaN:Mg samples.

In good agreement with the Doppler broadening results of Fig. 3.1, the positron lifetime spectra recorded in the MOCVD grown Mg-doped samples indicate strong evidence of vacancy defects (Fig. 3.2). Three positron lifetime components can be distinguished. The longest one has a value of $\tau_3 = 500$ ps ($I_3 = 6$ %), which is a typical lifetime for large open volume defects where more than 50 atoms are missing from their lattice sites (see Publ. [II]). The second lifetime component $\tau_2 = 180$ ps ($I_2 = 74$ %)is also larger than the lifetime in the lattice $\tau_B = 154$ ps indicating the presence of monovacancy defects. The shortest lifetime component is typically $\tau_1 = 90$ - 140 ps and corresponds to delocalized positrons annihilating in the GaN lattice. Its value is less than τ_B because it reflects both the annihilation and trapping of positrons. The annealings have a strong effect on the lifetime spectra by decreasing the intensity of I_2 and I_3.

The observation of the lifetime component $\tau_2 = 180$ ps is very interesting. This lifetime is clearly smaller than obtained previously for Ga vacancies (235 ps), indicating larger electron density and smaller open volume. The only possible candidates for such defects are N vacancies or complexes involving V_N. Further-

more, the lifetime of 180 ps is close to those expected for N vacancies according to theoretical calculations [11]. On the other hand, isolated N vacancy is not expected to be a positron trap because of its positive charge. This suggests strongly that neutral or negative complexes involving V_N are present in Mg-doped GaN.

The atoms neighboring the N vacancy can be experimentally identified by recording the momentum distribution of the annihilating core electrons, using the coincidence technique to measure the Doppler broadening spectrum [12]. The measurement was done at 550 K in order to maximize the positron trapping at the vacancy (Fig. 3.1). The lifetime experiments (Fig. 3.2), however, show that the measured Doppler spectrum $\rho(p)$

$$\rho(p) = \eta_B \rho_B + \eta_V \rho_V + \eta_{Cl} \rho_{Cl} \tag{3.1}$$

is a superposition of the momentum distributions in the lattice ρ_B, at V_N related defects ρ_V, and at larger vacancy clusters ρ_{Cl}. In order to decompose the Doppler spectrum, we calculate the positron trapping rates κ_V and κ_{Cl} from the measured intensities of the lifetime components τ_2 and τ_3, using the standard positron trapping model with two defects [7]. With the help of trapping rates the fractions of positron annihilations at the V_N complexes η_V=0.372 and at vacancy clusters η_{Cl}= 0.048 can be estimated in the as-grown sample at 550 K. The momentum distribution of the V_N complexes can be decomposed from Eq. (3.1) by recording ρ_B in MBE grown reference sample and ρ_{Cl} in MBE grown Si-doped GaN where vacancy clusters have been earlier observed (see e.g. Ref. [13] and Publ. [III]). Since the fraction of positron annihilations in the clusters is small, the possible error due to the inaccuracy of the cluster data is small.

The experimental core electron momentum distributions in the GaN lattice and in the N vacancy complexes are shown in Fig. 3.3. The curves have equal slopes, indicating that the dominant core electron shell is the same. The intensity of the distribution is smaller in the case of N vacancy complex, which is typical for an open volume defect. However, the intensity is larger than previously recorded for the Ga vacancy in GaN, supporting the identification of the V_N related defect.

A more detailed identification can be reached by comparison with theoretical calculations (Fig. 3.3). As shown earlier [12, 14], atomic wave functions can be used to obtain good quantitative agreement with the experimental core electron momentum distributions at momenta above 15×10^{-3} $m_0 c$. To mimic the experimental lattice distortions, the calculations were performed in a model structure where the atoms neighboring the vacancy were symmetrically relaxed in order to reproduce the experimental positron lifetime (180 ps for the V_N complex). The results show that Ga $3d$ core electrons are dominant both for annihilation in the bulk lattice and at N vacancy related defects, explaining the similar slopes of the experimental curves in Fig. 3.3. However, the intensity of the momentum
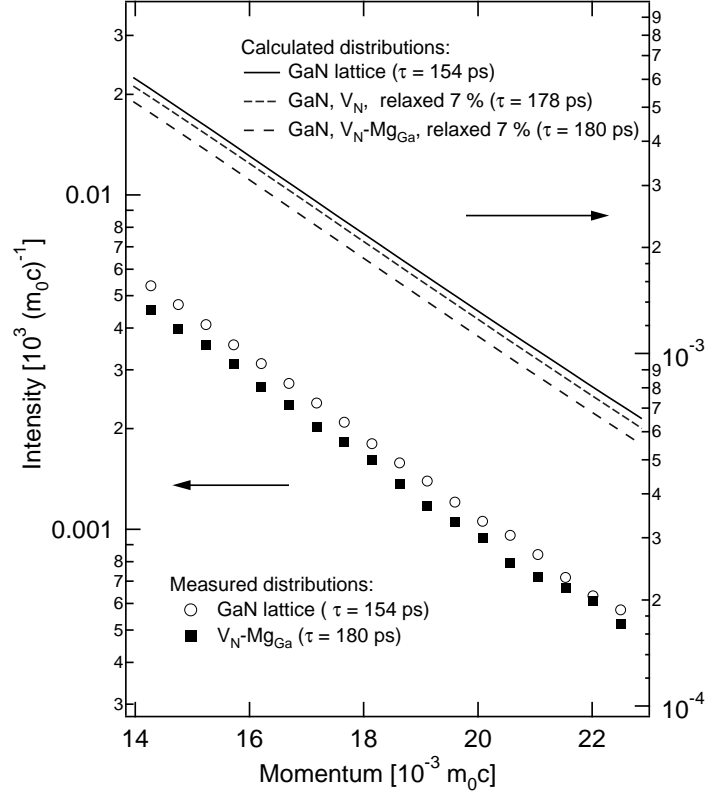
Figure 3.3: The measured and calculated momentum distribution curves.

distribution for isolated V_N is much too high. The conventional W parameter, calculated as the integral from Fig. 3 at $(15\text{-}20)\times10^{-3}$ m_0c and scaled to the lattice value W_B, is $W_{V_N}/W_B = 0.948$, which is much larger than the experimental result of $W_{rel} = 0.86(2)$. As expected from its repulsive positive charge, the isolated N vacancy is thus not the defect trapping positrons in Mg-doped GaN.

The low intensity of the experimental ρ_V suggests that one of the Ga atoms neighboring the N vacancy is replaced by an atom which does not have the Ga $3d$ core electrons. An obvious candidate is the Mg dopant atom, which has an opposite charge to V_N and thus may form a neutral V_N-Mg_{Ga} complex. In fact, the calculated momentum distribution for the V_N-Mg_{Ga} complex is in good agreement with the experimental one (Fig. 3.3). The relative W parameter is $W_{V_N-Mg_{Ga}}/W_B = 0.851$, which is the same as the measured $W_{rel} = 0.86(2)$ within the experimental accuracy. We can thus positively identify the native vacancy in the Mg-doped GaN as V_N-Mg_{Ga} pair.

The observation of V_N-Mg_{Ga} complexes in Mg-doped GaN is in good agreement with theoretical calculations, which predict a low formation energy ($\sim$1.4 eV) for such pairs [15–17]. According to theory the vacancy complexes involving either V_N or V_{Ga} should be the dominant defects at any position of the Fermi level during growth. The presence of Ga vacancy complexes [11] is well established earlier in n-type GaN. Confirming the theoretical prediction, the results of this work shows that V_N-Mg_{Ga} pairs exist in semi-insulating and p-type GaN.

3.2   The role of vacancy clusters in Mg-doped GaN

The studied samples in Publ. II were grown by metal-organic vapor phase epitaxy (MOCVD) on sapphire template (see Table 3.1) at Naval Research Laboratory, Washington D.C., USA. The magnesium concentration of samples varied between 0.25-9×10^{19} cm^{-3} and the [Si] = 0.13-8.4×10^{18} cm^{-3}. In addition, the sample #2 had a hydrogen concentration of 4×10^{18} cm^{-3} and [O] = 1×10^{17} cm^{-3}. Samples no. 3 and 4 were intentionally codoped with Si, the other samples have moderate Si concentration coming from the reactor walls during growth. The post-growth heat treatments were done by rapid thermal annealing (RTA) at 980 °C and in the case of Si co-doping at 1000 °C. As can be seen the Mg concentration is over two orders of magnitude higher than the hole concentration in sample #2. A p-type Mg-doped GaN sample grown by molecular beam epitaxy (MBE) was used as a vacancy free reference sample.

Figure 3.4 shows the S parameter as a function of incident positron energy in samples with different Mg concentrations. The reference level corresponding to the vacancy free lattice is shown with a dashed line. The annihilation from a bulk state gives the most broadened momentum distribution, which can be seen as a low S parameter. The vacancy free S parameter level as well as the bulk lifetime ($\tau_b = 160\pm 5$ ps) in GaN are well known on the basis of previous studies. Here we use a MBE GaN:Mg reference sample, which has the same positron lifetime as a defect free GaN lattice (see Sec. 3.1 and Publ. [III]).

In Fig. 3.4 the top axis shows the mean implantation depth of a positron related to the used acceleration voltage. The behavior of S parameter can be divided in three different regions: (1) Surface, (2) layer and (3) substrate. At low acceleration voltage (< 2keV) the penetration depth of positrons is low and they can diffuse back to the surface. At surface the electron density is reduced, and this leads to the more narrow annihilation line, which is seen as a high S parameter. At higher acceleration voltage (5-20keV) the S parameter characterizes the GaN layer. At even higher energies the S parameter is decreasing because the positrons are implanted to the sapphire substrate, where the electron momentum is higher. The

Table 3.1: The Mg and Si concentration measured by secondary ion-mass spectrometry in studied GaN layers in Publ. II. The hole concentrations were measured with Hall measurement [18] and in the case of reference sample with capacitance-voltage measurements. RTA stands for rapid thermal annealing and SITU means that samples were annealed in the growth reactor.

Sample number	Mg conc. $\times 10^{19} \text{cm}^{-3}$	Si conc. $\times 10^{17} \text{cm}^{-3}$	Hole conc. $\times 10^{17} \text{cm}^{-3}$	Annealing temp. $^\circ$C
#1	4.0	1.3	-	No anneal.
#2	4.0	1.3	1.7	980/RTA
#3	7.3	72	-	No anneal.
#4	9.0	84	-	1000/RTA
#5	1-2	5-6	-	800/SITU
#6	0.25	5-6	highly resistive	800/SITU
ref. [19]	-	-	$\sim$10	No anneal.

measured S parameter is hence a linear combination of individual S parameter of each region with respective weighting factors η_i (see Eq. 2.2).

To study the effect of Mg doping one has to concentrate to the region of 250-500 nm (Fig. 3.4). The sample containing the lowest Mg concentration has the same S parameter level as in bulk GaN. No vacancies are thus detected. On the other hand, the S parameter is $\sim$ 0.466 for the sample with Mg concentration of 1-2$\times 10^{19}$ cm^{-3}, and S $\sim$ 0.473 for sample #1 with highest Mg concentration. As can be seen the S parameter levels of samples have a clear order depending on the Mg content. The high S parameter is a finger print of vacancy type defect. At the vacancy the electron density is decreased and the annihilation line is more narrow giving higher S parameter than in the bulk lattice. Hence, positrons reveal increased trapping in vacancy type defects with higher Mg concentrations.

Figure 3.4 shows also the average lifetime τ_{ave} as a function of incident positron energy in the unannealed GaN:Mg sample measured at 300 K. At the surface the average lifetime is high due to the low electron density. τ_{ave} is lowest with positron energy of 2 keV and increases to the constant value of τ_{ave} = 185 ps in the range of 100-500 nm. As can be seen in Fig. 3.4 there is a region of lower vacancy concentration below the surface as seen also in the Doppler measurement.

The temperature behavior of the valence annihilation parameter S is shown in the Fig. 3.5. At elevated temperatures ($>$ 300 K) S parameters of samples #1 and #2 are clearly higher than those of the reference sample. At 600 K the S parameter of unannealed GaN:Mg sample reaches a value of S $\approx$ 0.513 and the
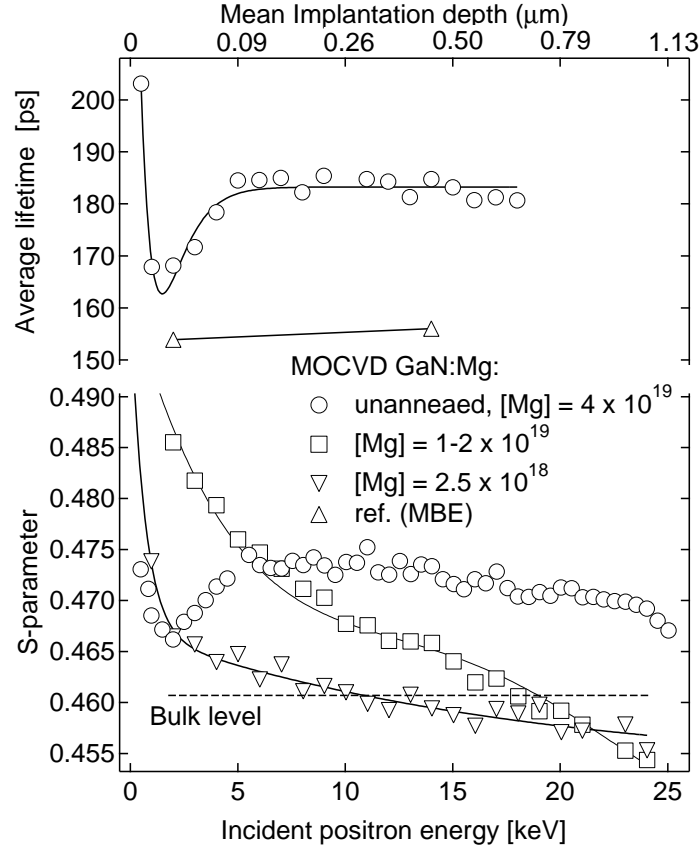
Figure 3.4: The average lifetime and S parameter as a function of incident positron energy. The samples were annealed at 800 °C except the one with highest Mg concentration. The dashed line represents the S parameter level of annihilations of delocalized positrons. The top axis indicates the mean implantation depth of incident positron. The solid lines are to guide the eye.

data in the annealed sample increase up to $S \approx 0.481$. Also the S parameters of co-doped samples are higher than that of the reference sample revealing positron trapping at the vacancies.

The samples have two competing positron traps based on the measurements as a function of temperature (Fig. 3.5). At low temperature the positrons get trapped by defects without open volume and thus less annihilations take place at vacancies. The candidate is the negative ion. The competing positron traps in Mg doped GaN are detected also in Publ. I, where the negative ion is attributed either to Mg_{Ga} acceptor or to a dislocation without open volume [9].
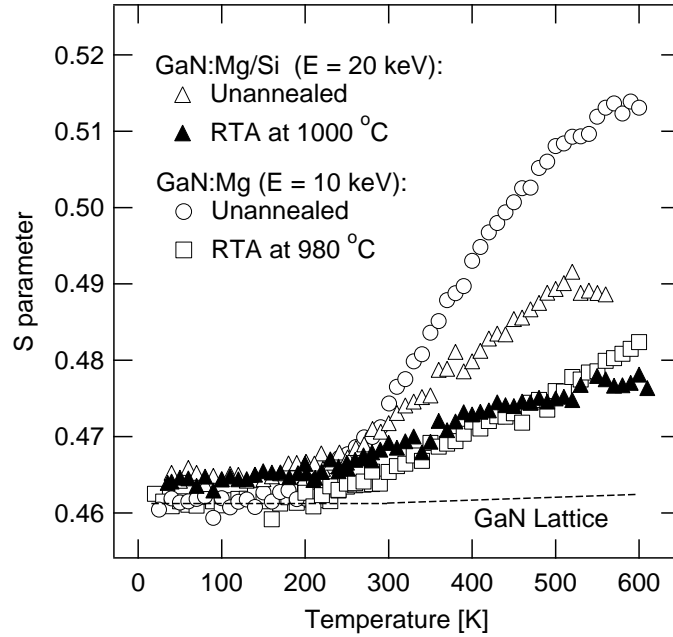
Figure 3.5: Valence annihilation parameter S as a function of measuring temperature. The incident positron energy was chosen high enough to make sure the annihilations arising from surface are excluded. The S parameter level for vacancy free p-type reference sample is indicated with dashed line.

To interpret the annihilation parameters independently of the vacancy concentration the core annihilation parameter W can be shown as a function of valence annihilation parameter S. Figure 3.6 shows the W vs. S plot measured in the annealed and unannealed sample. Both of these parameters were normalized with those measured for the GaN lattice. In the case of a single type of a vacancy defect, the measured S and W parameters fall on the straight line connecting the bulk value (S_b, W_b) and defect related value (S_d, W_d).

Figure 3.6 shows the characteristic S and W parameters for gallium vacancy (V_{Ga}) as obtained in Ref. [11]. The slope of S-W plot for the as-grown sample #1 is almost the same as measured before [13] for vacancy cluster. Furthermore, the slope of S-W plot is constant, which means that a single vacancy defect type dominates the Doppler broadened spectrum. The change in relative S parameter ($S/S_b \sim 1.1$) of the unannealed sample is typical for vacancy clusters and much larger than expected for monovacancies.

After annealing the change in the relative S parameter is more moderate ($S/S_b \sim 1.045$). This S parameter is close to those determined for the native Ga vacancy
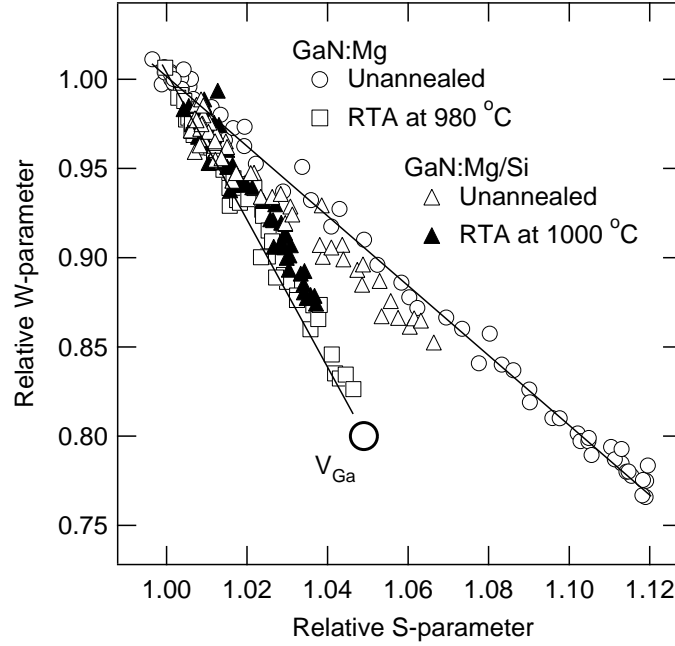
Figure 3.6: The core annihilation parameter W as a function of valence annihilation parameter S measured at different temperatures in order to enhance the trapping at vacancies. V_{Ga} represents positron annihilations at Ga vacancy. Note, that the data is the same as in Fig. 3.5.

[11]. Again the slope is constant indicating a single dominant vacancy defect type. However, the slope differs from the one before annealing, which shows that the type of vacancy defect changes. Since the (S,W) parameter becomes closer to those of V_{Ga}, we conclude that the size of the vacancy cluster decreases in annealing.

The co-doping of GaN:Mg samples with Si atoms generates also vacancy type defects as can be seen in Fig. 3.5. Before annealing they have the characteristic slope in S-W plot (Fig. 3.6) revealing the existence of vacancy clusters. We conclude that the annealing changes the slope, similarly as in the Mg doped samples #1 and #2. The annealing makes these clusters to convert to smaller size vacancy defects with annihilation parameters close to those of V_{Ga}.

In the unannealed sample #1 three different lifetime components are found. The smallest is $\tau_1 \approx 70$ ps which is related to positron annihilations in the delocalized state. In the presence of open volume defects the lowest lifetime is clearly smaller than the bulk lifetime because of the trapping.

The spectrum of unannealed GaN:Mg measured at 14 keV reveals high intensities of two vacancy related lifetimes. The lower is $\tau_2 = 180$ ps and the higher $\tau_2 = 435$ ps. The shorter lifetime $\tau_2 = 180$ ps is the same as reported in Publ. I, where the $\tau_2 = 180$ ps is connected to the V_N-Mg_{Ga}-complex. The longer lifetime component $\tau_3 = 435$ ps is so high that it cannot arise from single mono vacancies. The lifetime of 435 ps is hence attributed to a vacancy cluster. It has been shown that the positron lifetime at vacancy clusters is sensitive to the size of the clusters [20,21]. To estimate the open volume size of the vacancy cluster with the positron lifetime of 435 ps we calculate the positron lifetimes theoretically. For the positron states we use the conventional scheme with the local density approximation (LDA) for electron-positron correlation effects and the atomic superposition method in the numerical calculations [22,23]. The positron annihilation rate λ is

$$\tau^{-1} = \lambda = \pi r_0^2 c \int d\boldsymbol{r} |\psi_+(\boldsymbol{r})|^2 n_-(\boldsymbol{r}) \gamma[n_-(\boldsymbol{r})], \qquad (3.2)$$

where n_- is the electron density, $\psi_+(\boldsymbol{r})$ the positron wave function, r_0 the classical electron radius, c the speed of light and γ is the enhancement factor, for which we use the interpolation by Boronski and Nieminen [24]. The positron state was solved in a 216 atom super-cell, in vacancy clusters up to the size of 62 missing atoms (Fig. 3.7).

As can be seen in Fig. 3.7 the positron lifetime starts to saturate above 400 ps when the cluster includes more than 30 V_{Ga}-V_N vacancy pairs. This is the consequence of the reduced electron density at the annihilation site. The solid line in Fig. 3.7 presents the annihilation rate

$$\lambda = \tau^{-1} = (2 + A e^{-Bn^{1/3}} + C e^{-Dn^{1/3}}) \times 10^9 s^{-1}. \qquad (3.3)$$

The electron concentration n is inversely related to vacancy size N and $A - D$ are fitting parameters. The function has a saturation lifetime at 500 ps, which is the lifetime of the negative positronium atom, similarly as in the Brandt-Reinheimer formula [25].

The electron density in a vacancy cluster plays a crucial role when determining the annihilation rate of a positron. We motivate the Eq. 3.3 in the following way. Ga atom is much bigger than N, and the positron probes mainly the electron density of a Ga atom. The electron density of Ga atom decreases exponentially with the radial distance r $\propto$ N$^{1/3}$. At small cluster sizes positrons annihilate with both Ga ($4s$,$4p$) valence electrons and Ga ($3d$) core electrons. In larger vacancy clusters the annihilation with the valence electrons strongly dominates. Hence, the fitted sum of two exponent functions can be thought as an annihilation with two different electron shells, which is controlled by the size of the vacancy cluster. As seen in Fig. 3.7, the simple scaling of Eq. 3.3 reproduces very well
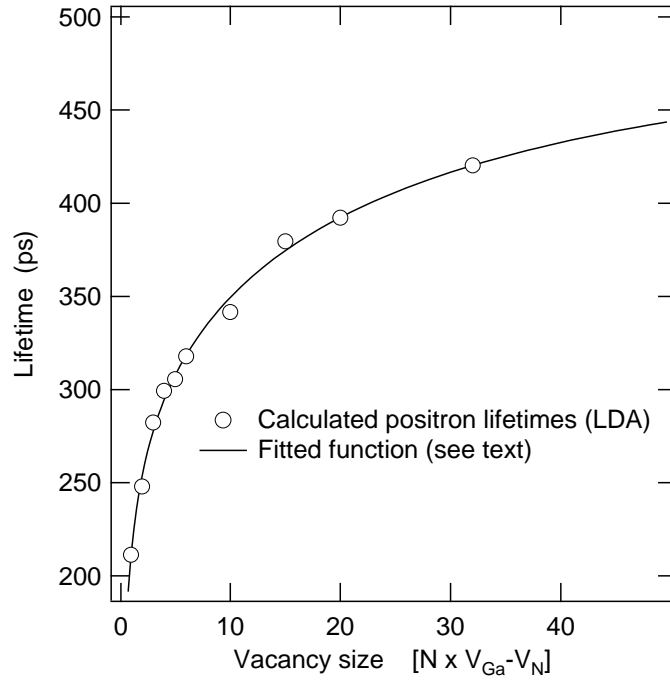
Figure 3.7: The calculated positron lifetime as a function of the number of vacancy pairs. The solid line is a fit of a function, where electron density n is inversely related to the vacancy cluster size.

the positron lifetimes calculated with atomic superposition method (Eq. 3.2). The result of Fig. 3.7 is quantitatively similar to the behavior of the calculated positron lifetime in Fe vacancy clusters [26]. This means that the number of missing Ga atoms determines the positron lifetime.

The experimental positron lifetime of 435 ps is close to the saturation of the curve of Fig. 3.7, but yet smaller than the $n \to 0$ limit of 500 ps of the Brandt-Reinheimer formula [25]. Experimentally the lifetime of 500 ps has been observed in other GaN:Mg samples [I], as well as in deformed Si [27] or GaAs [26]. These comparisons suggest that the lifetime of 435 ps is not yet in saturation as a function of the vacancy cluster size. We thus attribute it to clusters where about 60 atoms (30 GaN molecules) are missing (cluster radius of about ~ 5 Å).

Chapter 4

Native defects in oxygen, carbon and silicon doped GaN

The doping of semiconductor is a fundamental process controlling the free charge carrier densities. While the p-type doping of GaN has turned out to be difficult n-type material is easy to achieve. After growth GaN is usually n-type because of the high concentrations of residual impurities. This may not be the case in molecular beam epitaxy (MBE) growth which is done in high vacuum to reduce the impurity concentration. The n-type doping is usually done with oxygen or silicon atoms. In n-type GaN the Ga vacancy has the lowest energy to form. It is one of the most studied defects in GaN. However, the previous experiments have not succeeded to distinguish directly between the isolated Ga vacancies and complexed V_{Ga}.

In the next section we concentrate to the n-type doping of GaN. We show that the positron-electron momentum distribution is sensitive enough to distinguish the isolated Ga vacancy from the V_{Ga}-O_N-pair [V]. The investigation of C doped semi-insulating GaN reveals increasing yellow luminescence without the presence of Ga vacancies [IV]. The vacancy cluster formation in Si doped and mass transport GaN is studied in the Publ. [III] and [VI].

4.1   Ga vacancies in oxygen doped layers

The formation of V_{Ga} is usually related to high oxygen content of the GaN sample. It is shown that the Ga vacancies are the most common defects in oxygen doped MOCVD GaN [28] as well as in HVPE GaN [9]. In Publ. V we have studied the effect of controlled O doping to the vacancy type defects. The annihilation curve

obtained in electron irradiated GaN differs from O doped HVPE GaN revealing changes in the chemical neighborhood of the Ga vacancy. This shows that Ga vacancy is complexed with O atoms in O doped samples.

The measured free standing n-type GaN samples with different levels of intentional oxygen doping were grown by hydride vapor phase epitaxy (HVPE) at CREE laboratories. The free electron and oxygen concentrations were measured with Hall and SIMS methods, respectively, and they can be found in Fig. 4.1. The sample thicknesses varied between 350-810μm. To create a reference sample with isolated Ga vacancies, the irradiation of an undoped GaN sample with 2 MeV electrons at 300 K to a dose of 5×10^{17}e$^-$cm^{-2} was done at Wright State University, USA.

Fig. 4.1 shows the positron average lifetime as a function of measuring temperature. The positron lifetime in undoped GaN is 160-163 ps. This is the same as the lifetime in the GaN lattice [8, 11] indicating low native vacancy concentrations. As can be seen in Fig. 4.1 the measured average lifetimes in O doped HVPE GaN are clearly higher than the lattice lifetime τ_b for all the samples over the whole temperature range. In decomposition two different lifetimes are found, where the longer one is $\tau_2 = 235 \pm 5$ ps. This is the same as measured before for gallium vacancy [11, 28]. The another lifetime component is $\tau_1 \approx 130$ ps. This is shorter than the lattice lifetime reflecting both annihilation and trapping from the delocalized state.

The average lifetime increases when the measuring temperature is decreased (Fig. 4.1). This kind of temperature behavior of the average lifetime is the fingerprint of negatively charged vacancies. Because of the Coulombic nature of the free positron wave function the trapping at vacancies enhances as the thermal velocity of the positron decreases [29, 30]. No other negative centers compete with the Ga vacancy in positron trapping. Negative ions, for example, would localize positrons in a hydrogenic state at low temperatures, strongly decreasing the fraction of annihilations at vacancies and the average lifetime at low temperatures [8]. The positron data thus show that the Ga vacancy related defects are dominating negatively charged acceptors. This has been demonstrated before in nominally undoped GaN, [31] but the present data show the dominant role of V$_{\mathrm{Ga}}$-related defects over four orders of magnitude of O doping.

The vacancy concentration can be estimated from the measured lifetimes. Since one vacancy type defect is present, the vacancy concentration is obtained as [29]

$$c_V = \frac{N_{at}}{\mu_V \tau_b} \frac{\tau_{ave} - \tau_b}{\tau_D - \tau_{ave}}, \tag{4.1}$$

where N$_{at}$ is the atomic density, τ_b=160 ps is positron lifetime in the GaN lattice, μ_V=7$\times10^{15}$ at. s^{-1} is positron trapping coefficient at the vacancy, and $\tau_D = 235$
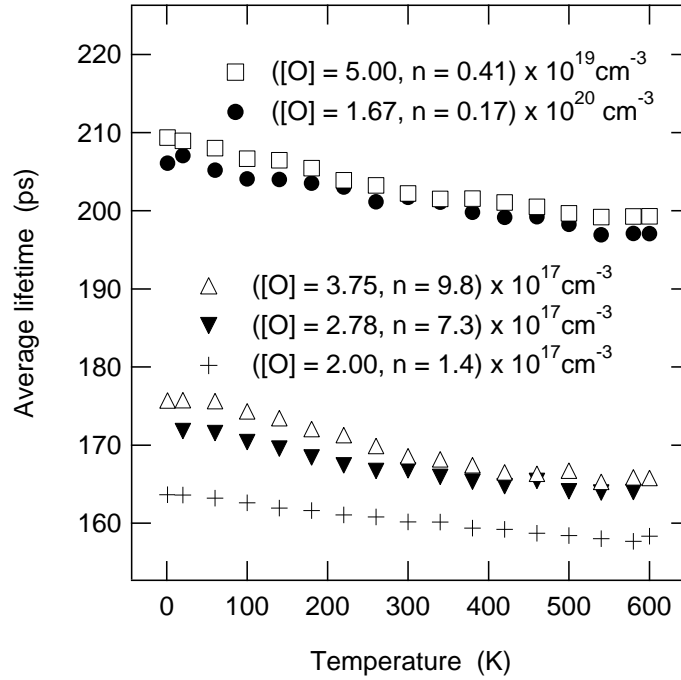
Figure 4.1: Measured average positron lifetime as a function of measuring temperature. Note, that the first number in the parentheses stands for O concentration and the second one for the free carrier concentration, which were measured at 300K.

ps is the positron lifetime at the Ga vacancy. As can be seen from Fig. 4.2 the increase of the O doping of the samples increases the V_{Ga} concentration. This trend is theoretically predicted for acceptor defects like V_{Ga}, [6] and suggests that the gallium vacancy is complexed with oxygen atom. However, the positron lifetime is too insensitive to tell if the V_{Ga} is isolated or complexed.

In order to identify an intrinsic Ga vacancy we studied an electron irradiated undoped GaN sample (2 MeV, $5 \times 10^{17} e^- cm^{-2}$). The average positron lifetime is 205 ± 3 ps at 380 K. The slightly higher measuring temperature was chosen to introduce maximal trapping at vacancies and minimize the effect of negative ions. The decomposition of the lifetime spectrum of electron irradiated GaN reveals a Ga vacancy related lifetime 230 ± 5 ps, i.e. the same as in O-doped HVPE GaN. The concentration of Ga vacancies is $5 \times 10^{17} cm^{-3}$ (Eq. 4.1). Electron irradiation (2-MeV) of GaN samples thus generates intrinsic Ga vacancies with an introduction rate of 1 cm^{-1} by removing the Ga atoms from the lattice sites to the interstitial sites [10]. The introduction rate of 1 cm^{-1} is typical for primary defects formed in electron irradiation. The oxygen concentration of irradiated
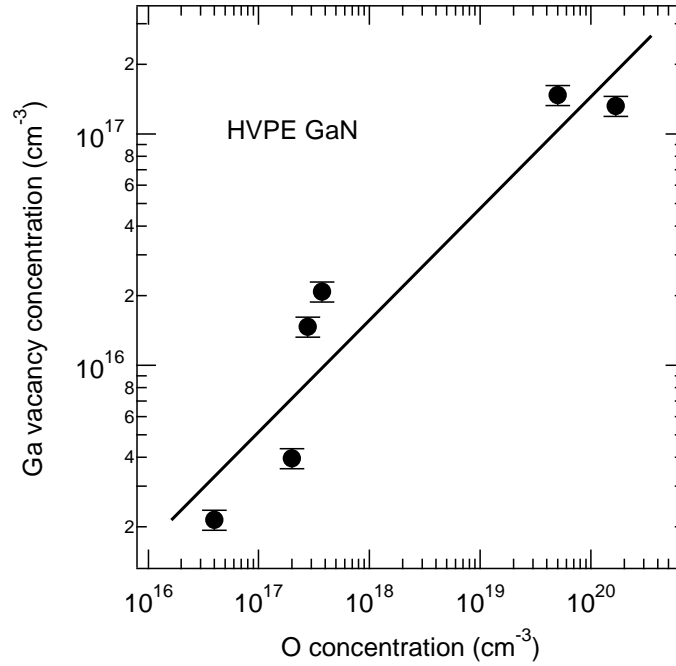
Figure 4.2: Gallium vacancy concentration as a function of doping. The solid line is to guide the eye. The results for the sample with the lowest O concentration have been taken from Ref. [31].

GaN is two orders of magnitude lower than the gallium vacancy concentration. We conclude that positrons are trapped at isolated Ga vacancies in the irradiated GaN sample.

The experimental results were compared with ab initio calculations as described in Publ. V. The behavior of the calculated annihilation curves correlate well with the experimental curves through the whole momentum range (Fig. 4.3). Especially in the case of the isolated Ga vacancy the annihilation lines are almost the same in the experiment and theory, supporting the identification of the isolated Ga vacancy. The main contribution in the range between $10\text{-}30 \times 10^{-3}m_0$c arises from annihilations of Ga $3d$ electrons. The decrease in intensity at this momentum region is due to the reduced intensity of Ga $3d$ electrons in a Ga vacancy. The good agreement at both valence and core electron regions manifests the accuracy and predictive power of the theoretical calculations.

Fig. 4.3 shows the measured electron momentum distributions in various GaN samples having Ga vacancy related defects. The curves are not similar, which indicates that different complexes can be distinguished. In the momentum range
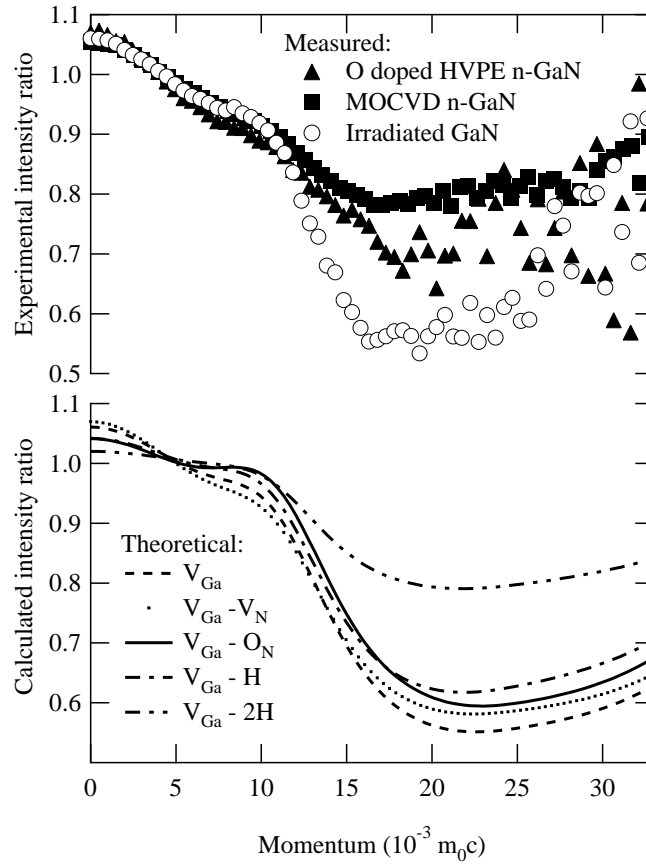
Figure 4.3: Measured and calculated momentum distribution curves for different types of samples and defects, respectively. All of these curves were normalized to the curve obtained from bulk GaN.

between 15-30×10^{-3}m$_0$c the samples have a clear order. The intensity of irradiated GaN is the lowest while the oxygen doped GaN has higher intensity. The difference between irradiated and O doped GaN is interesting. While electron irradiation generates isolated Ga vacancies, the O doping increases the native Ga vacancy concentration (Fig. 4.2) which suggests a formation of V$_{Ga}$-O$_N$-pairs in growth. In Fig. 4.3 the O doped HVPE GaN has higher relative intensity in high momentum region when compared to electron irradiated GaN. This effect could be attributed to oxygen surrounding the Ga vacancy: O is a smaller atom than N and thus contributes more at high electron momentum. The same behavior can be seen in calculated momentum ratio curves. The difference between V$_{Ga}$-O$_N$ and isolated V$_{Ga}$ is arising from the valence electron states derived from the atomic $2p$ orbitals. Although the electron densities around O and N nuclei are almost

Table 4.1: The positron annihilation parameters and defect related lifetimes for studied samples and defects.

	τ_V [ps]	S_V/S_b	W_V/W_b
Experimental:			
Irr. V_{Ga}	230(5)	1.042(3)	0.58(3)
HVPE V_{Ga}	235(5)	1.050(3)	0.73(3)
MOCVD V_{Ga}	-	1.039(3)	0.80(3)
GaN lattice	160(3)	1	1
Theoretical:			
V_{Ga}	200	1.048	0.583
V_{Ga}-V_N	203	1.055	0.608
V_{Ga}-O_N	200	1.032	0.630
V_{Ga}-H	180	1.034	0.642
V_{Ga}-2H	155	1.017	0.803
GaN lattice	131	1	1

the same the difference between the curves is clear.

Table 4.1 shows the calculated annihilation parameters for the studied samples and defects. Calculated positron lifetimes are shorter than the experimental ones, but the lifetime differences between the Ga vacancy and lattice are the same, $\tau_V - \tau_b \approx 70$ ps. The experimental and theoretical annihilation parameters (Table 4.1) are in good agreement in the case of an isolated Ga vacancy. The remaining discrepancies are in the limits of the accuracies of both experimental and theoretical methods. The increase of W parameter due to O decoration is clear in the experiment and theory, which provide direct evidence that V_{Ga}-O_N complexes are formed in the oxygen doping of HVPE GaN. However, the S parameter in O-doped GaN is higher than the calculated value for V_{Ga}-O_N. This could indicate that V_{Ga}-V_N divacancies are present, as predicted by the low calculated formation energy of such defects [6, 32]. The presence of divacancies is also supported by the slightly higher positron lifetime at vacancies in O-doped than in irradiated GaN. The high value of W_{rel} (Table 4.1) shows that the divacancies are likely to be decorated with oxygen.

The GaN grown by metal-organic chemical vapor deposition is the most important for optoelectronic applications. In this material the concentrations of residual impurities, especially of hydrogen, are high due to organic precursors applied in the growth. The electron momentum distribution at V_{Ga}-related defect (Fig. 4.3 and Refs. [11] and [19]) is different from both V_{Ga} and V_{Ga}-O_N. To explain the data in MOCVD GaN at high momentum region, we performed a calculation in

Ga vacancy related defects containing 1-2 hydrogen atoms (Fig. 4.3). H pushes the positron density out from the vacancy leading to a shorter lifetime and a higher intensity ratio at the high momentum region (Table 4.1). The experimental curve measured in MOCVD GaN is close to the calculated one at V_{Ga}-H or V_{Ga}-2H complexes, suggesting that the Ga vacancy in MOCVD GaN is decorated by hydrogen or possible also by oxygen. Such complexes have low formation energies according to calculations [33, 34].

4.2   Ga vacancy relation to "yellow luminescence" in C-doped GaN

An important deep-level phenomenon in GaN is the yellow luminescence (YL) band, the origin of which has been a subject of some debate. Neugebauer and Van de Walle has argued that V_{Ga} is most likely the deep level responsible for YL [35]. The YL was attributed to a transition between a shallow donor (Si_{Ga} or O_N) and a deep acceptor V_{Ga}. The intensity of YL correlates with the concentration of Ga vacancies in n-type GaN. Although there is much support for the shallow donor-V_{Ga} model in n-type GaN, it cannot account for all of the experimental results in insulating GaN, where the large body of evidence is linking the YL intensity with carbon concentration [36–41]. From defect formation energy arguments, the V_{Ga} concentration should be negligibly small in SI GaN, an apparent contradiction given the strong YL observed. To solve these discrepancies the model of two different defects involved in YL has been proposed, one of them being carbon related [42]. In Publ. IV we have studied the vacancy signal obtained from SI GaN:C. The investigation shows that the defect behind YL differs from V_{Ga} in C doped SI GaN.

A series of 1 μm thick GaN films doped using CCl_4 as a carbon source was grown by dc plasma-assisted molecular-beam epitaxy (MBE). Growth was performed in Ga-rich conditions at 750 °C on semi-insulating ($\sim 10^9$ Ω-cm) GaN templates grown on c-plane sapphire by metal organic vapor phase epitaxy (MOVPE). Further details have been reported previously [40]. The dislocation density estimated by asymmetric x-ray rocking curves is in the mid-10^9 cm^{-2}. No degradation of the rocking curves was observed for carbon doping levels up to the mid-10^{18} cm^{-3}. The growth and sample characterization were done at University of California, Berkeley, USA.

In Fig. 4.4, the data for SI GaN:C coincide with the S parameter for GaN without positron trapping at vacancies (measured in a p-type GaN:Mg reference sample [I]). Thus, the V_{Ga} concentration in the carbon-doped films is below the detection limit ($< 10^{16}$ cm^{-3}) [29]. In contrast, the n-type reference film shows an increased
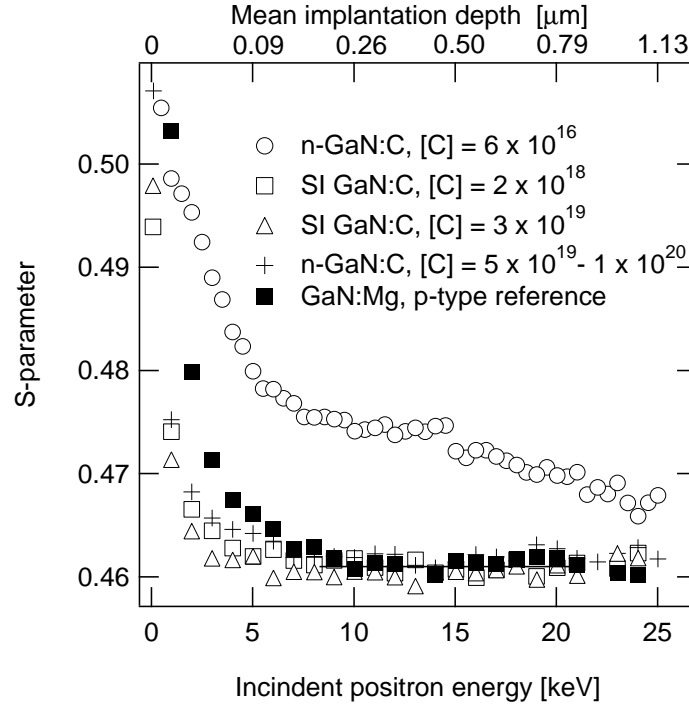
Figure 4.4: The low electron momentum parameter S as a function of implantation energy for C doped GaN samples. The top axis indicates the mean stopping depth of positrons.

S parameter indicating that a fraction of the implanted positrons annihilate at vacancies. These vacancies were tentatively attributed to V_{Ga} in Publ. IV, but by studying the linearity of a S-W plot (Fig. 4.8) the vacancy defect is more likely a cluster of several monovacancies.

The V_{Ga} concentration of the GaN:C layer is below detection limit, but the layer shows a high absolute integrated YL intensity. The most likely explanation is that shallow donor-V_{Ga} recombination is not the only mechanism for YL in GaN, and a carbon-related mechanism also exists. In other words, a transition involving carbon deep levels happens to have approximately the same luminescence energy as the V_{Ga} transition causing YL in n-type GaN.

4.3 Vacancy clusters in Si-doped MBE GaN

The high-growth rate of HVPE grown GaN enables rapid fabrication of thicker films where the concentrations of impurities, as well as point and extended de-
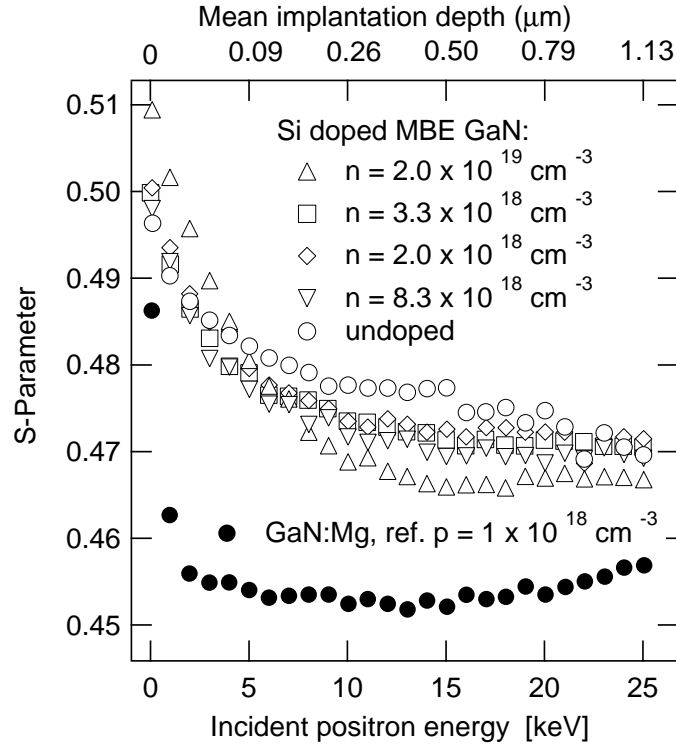
Figure 4.5: The low momentum parameter S as a function of incident positron energy. The reference level corresponds to annihilations in defect free lattice.

fects, are reduced. Even lower impurity concentrations of grown GaN samples can be achieved by utilizing the clean growth environment of molecular-beam epitaxy (MBE). Compared with the extensively studied MOCVD GaN on sapphire, much less is known on the properties of MBE GaN especially when grown homo-epitaxially on the HVPE GaN substrates. In Publ. III the characterization of vacancy type defects in Si doped MBE GaN on HVPE GaN substrate is done. The study reveals significant concentrations of monovacancies as well as vacancy cluster type defects.

The samples were grown using an MBE system equipped with a nitrogen rf-plasma source at Tampere University of Technology, Finland. The substrate was HVPE-grown GaN (~ 6 μm)/sapphire (0001) template. The dislocation density in such HVPE GaN is about 10^9 cm^{-2}. The films were grown at 800 °C under 7×10^{-5} mbar nitrogen background pressure at rf-power of 400 W. Temperature of the silicon cell was varied between 1150 and 1300 °C to prepare GaN with different doping levels. A few undoped and Mg-doped p-type GaN samples were

also grown. The layer thickness was 1.5 μm and the growth rate 0.5 μm/h.

Figure 4.5 shows the S parameter values measured at room temperature as a function of the positron incident energy in undoped, Mg-doped (p$\sim$1$\times$10^{18} cm^{-3} by electrochemical capacitance measurement), and Si-doped layers. At high-incident energies the S parameter settles down to constant level, which characterize the annihilations inside each MBE GaN. The average penetration depth with the highest-positron implantation energy, 25 keV, is about 1.13 μm in GaN. Hence, the effect of the underlying HVPE GaN layer can be seen in the Mg-doped sample, as the S parameter starts to increase slightly at E > 20 keV. The S parameter level characterizing the MBE layer can be determined at positron energies between 10 and 20 keV for Mg-doped layer and between 15 and 20 keV for undoped and Si-doped layers.

The S parameter characterizing the MBE GaN is the lowest in Mg-doped sample and clearly higher in Si-doped and in undoped samples. The reference level in Fig. 4.5 is determined by Doppler broadening and positron lifetime measurements in GaN:Mg single crystal and by lifetime experiment with pulsed positron beam [I]. The S parameter measured in the undoped layer and in Si-doped layers is clearly higher than the reference level indicating that the positrons are trapped at vacancy-type defects in these layers. The relative S parameter S/S_b is between 1.031 and 1.045 in undoped and Si-doped layers. The vacancy specific S parameter S_V/S_b for the Ga vacancy in GaN has been determined by comparing the Doppler broadening and positron lifetime measurements, to be 1.046 for the current detector system [19]. The change in S parameter is too big to be characteristic for the N vacancy.

The most probable candidate for the vacancy-type defect observed in the films is a vacancy cluster of two or more vacancies. The formation of vacancy clusters has been previously found in MBE-grown GaN on Si(111) substrate [13], where the formation of the vacancy clusters was suggested to be related to Si and Ga inter-diffusion processes during the growth. The characteristic (S,W) values for the vacancy cluster in Ref. [13] were estimated to be 1.10$\times$S$_b$ and 0.75$\times$W$_b$, thus clearly above the line characterizing the gallium vacancy in the S-W plane (see Fig. 4.8). Any presence of Ga monovacancies in MBE-grown GaN cannot be totally excluded, despite the fact that post-growth heat treatment should have eliminated all mobile defects. One cannot rule out the possibility that S and W are actually superpositions of three states, namely, annihilation of free positrons in the GaN lattice, positrons trapped at vacancy clusters, and the positrons trapped at Ga monovacancies.

Positron annihilation results in the n-type GaN layers reveal positron trapping at vacancy clusters. Their concentration decreases with increasing [Si]. Although the present data do not allow accurate distinction between the vacancy clusters
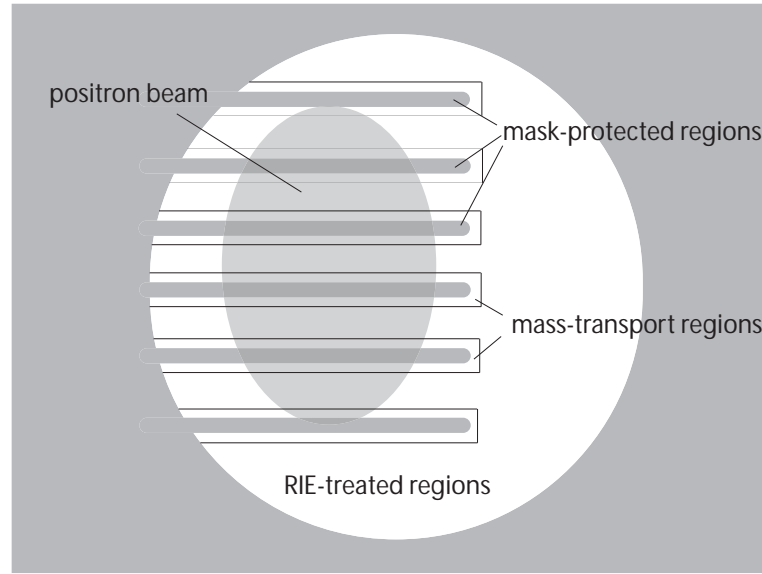
Figure 4.6: Schematic presentation of the structure of the MT grown GaN samples. The oval region illustrates the size of the positron beam. About 10-30 % hit the MT-region.

and the Ga monovacancies, the positron annihilation and PL results [III] suggest that also V_{Ga}-donor impurity complexes are present in the Si-doped layers in addition to vacancy clusters.

4.4 Vacancy type defects in the mass transport grown GaN

Because of the extreme conditions needed for the growth of bulk GaN, the epitaxial methods have proved to be more convenient way to produce GaN samples. In epitaxially grown GaN layers the dislocation density is high because of the lattice mismatch with the substrate. Several laterally epitaxial overgrowth (LEO) methods [43,44] have decreased the dislocation density to the levels of even as low as 10^4-10^5 cm^{-2} [45]. However, a spatially resolved study of defect distribution and optical properties of the LEO structures revealed an increase of the dopant incorporation in the overgrown regions [46] due to the presence of a foreign mask material, which also introduces a local strain pattern. Recently, Nitta et al. [47,48] have demonstrated a technique of mass transport (MT) over GaN trenches during high-temperature annealing of line-patterned GaN in a metal-organic vapor-phase epitaxy (MOCVD) growth chamber that allows lateral growth and thus also leads
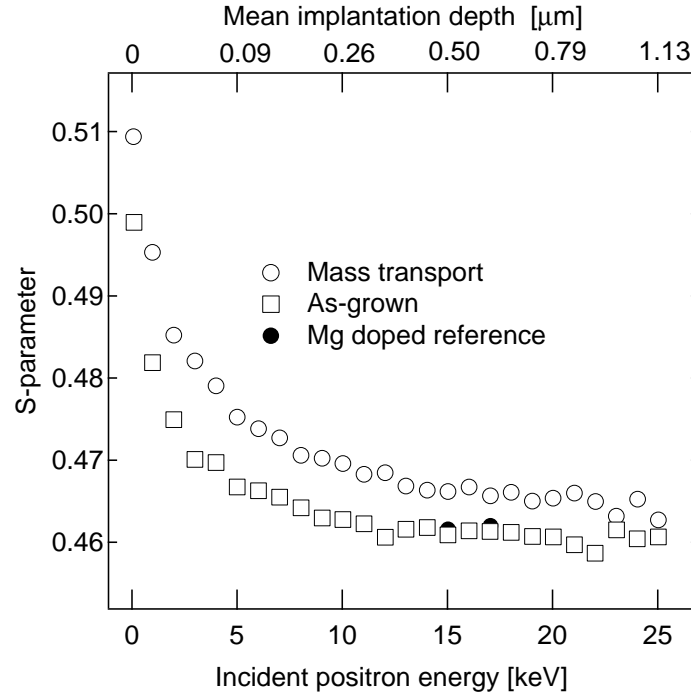
Figure 4.7: The low electron momentum parameter S as a function of incident positron energy. The as-grown sample indicates the S parameter level of a sample before mass transport growth.

to a bending of the dislocations.

The initial GaN layer used for the MT structure was deposited by HVPE on sapphire at a temperature of 1080 °C at the University of Linköping, Sweden [VI]. The thickness of the as-grown layer was 10 μm and the electron concentration at room temperature was around 3×10^{17} cm^{-3} [49]. Patterning of a 1000-Å-thick SiO$_2$ mask was achieved using standard photo-lithography techniques. Micrometer-sized trenches were patterned on the GaN surface by reactive ion etching (RIE). Three areas with different trench/spacing widths (10×5 μm, 25×5 μm and 25×10 μm), and depth of about 2 μm were prepared. After the RIE process, the traces of the SiO$_2$ mask were removed in a chemical solution. The structure was annealed at 1080 °C in an atmosphere of 40 % ammonia in nitrogen gas. During the annealing, a lateral MT GaN growth occurred around the barriers although no group-III source gas was supplied.

The S and W parameters were measured at 300K as a function of the positron beam energy E (Fig. 4.7). At high energies of E>10 keV; the S(E) and W(E)
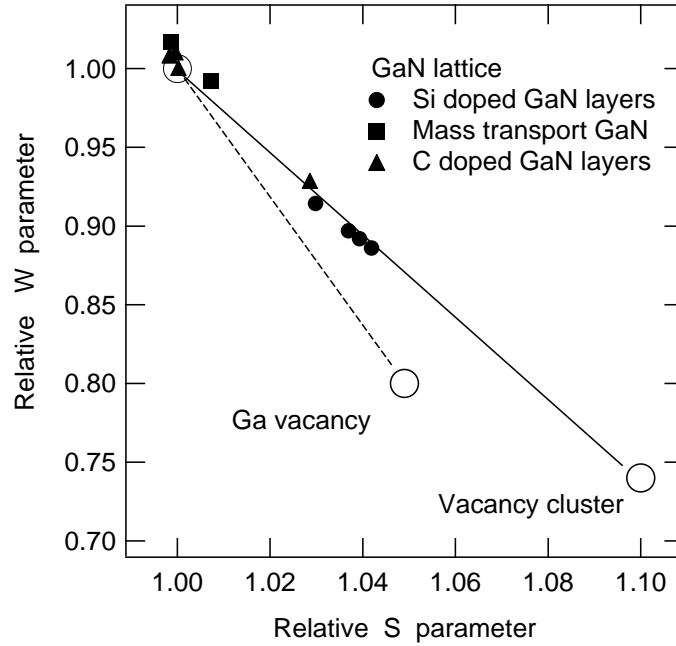
Figure 4.8: The high electron momentum parameter W as a function of low momentum parameter S measured from GaN samples with different doping content and growth methods.

curves saturate, which indicates that no positrons diffuse to the surface. The S and W parameters measured at E = 15-25 keV scan a depth of 0.5-1 μm below the surface. Since the diameter of the positron beam is about 1 mm, the measured data represent an average of the masked and MT regions (Fig. 4.6).

The S parameter of the as-grown HVPE sample is the same as in the MOCVD grown GaN:Mg sample, which is used as a reference since it contains no vacancy defects capable of positron trapping [28]. The as-grown HVPE sample thus has no detectable concentration of vacancies. On the other hand, the MT sample has a clearly higher S parameter, which indicates the formation of vacancy defects in the MT regions. Since this region covers only 10-30 % of the sample surface area, the increase of the S parameter is very significant.

The dependence between the measured S and W parameters yields information on the identity of the vacancy defects [29]. Such analysis is presented in Fig. 4.8, using the data measured at E = 10-25 keV to avoid the surface effects. The (S,W) points fall clearly off the line characteristic of the Ga vacancy identified earlier [10, 11]. On the other hand, the data fits well with the line previously associated to vacancy clusters formed in MBE grown GaN samples [III] [50].

Instead of simple point defects like V_{Ga} and V_{Ga}-O_N, the MT region thus contains empty vacancy clusters where several Ga and N atoms are missing. In order to induce the effect seen in the S and W parameters (Figs. 4.7 and 4.8), the vacancy cluster concentration must be in the 10^{16}-10^{17} cm^{-3} range in the MT regions.

The formation of clusters could be a consequence of the different growth velocities in the different growth directions during the conventional and lateral MT growths, perhaps enhanced also by the high impurity concentration present in the MT region. Having in mind the improbability for creating stable isolated Ga vacancies at the high annealing temperature used for MT growth of 1080 °C [10], as well as the results from SIMS spatial analysis showing a significant increase of O impurity in the MT area, we attribute the defects to a vacancy complex involving Ga vacancies and oxygen V_{Ga}-O-X.

Chapter 5

Summary

In this work the influence of doping to the epitaxial layers of gallium nitride has been studied by positron annihilation spectroscopy. The variable energy positron beam was used for Doppler measurements. Some samples were also characterized using a pulsed positron beam for lifetime experiments. Also the conventional lifetime measurements were done for the thick O doped HVPE GaN samples.

Nitrogen vacancies were found in significant concentrations in semi-insulating Mg doped GaN layers grown by MOCVD. Isolated V_N is positively charged and does not trap positrons. It is shown that N vacancies are neutralized by Mg acceptors by forming V_N-Mg_{Ga}-complexes. The lifetime of a positron in V_N is distinguishable from the bulk lifetime as well as from the lifetime of the Ga vacancy. We further show that high Mg content can introduce a large number of vacancy clusters. These defects form a inhomogeneous depth profile, where a lower vacancy concentration is found in a layer below the surface. The vacancy type defects in p-type GaN are important compensating centers limiting the free carrier concentration.

The n-type doping of GaN can be done with O or Si atoms. The O doping generates Ga vacancies with concentrations following the O content. The result presented here indicate that vacancies form complexes with O atoms. We show by comparing O-doped and electron irradiated GaN, that the Doppler broadening experiment is sensitive enough to distinguish between isolated V_{Ga} and V_{Ga}-O_N complex. Because of the reduced atomic radius of the O atom the electron density at the neighborhood of the Ga vacancy is slightly increased which leads to the broadened momentum distribution of the annihilating positron-electron pairs.

Si-doped GaN samples grown by molecular beam epitaxy were found to contain a significant amount of vacancy clusters. The concentration of the clusters is

decreased with increasing Si content. Evidence of monovacancy complexes such as V_{Ga}-Si_{Ga} was also obtained.

In n-type GaN yellow luminescence (YL) is connected to the energy level introduced by Ga vacancies. Carbon doping was found to decrease the concentration of both free electrons and Ga vacancies, but to enhance the intensity of the yellow luminescence. We conclude that the interstitial carbon contributes to the YL emission when its concentration exceeds that of Ga vacancy.

To decrease the density of dislocations in epitaxially grown GaN layers the lateral overgrowth methods are used. We studied the defect formation by lateral growth in a mass-transport GaN sample. The results show that the overgrowth generates vacancy clusters, in correlation with an increase in the impurity concentration.

Bibliography

[1] D. Schödlbauer, P. Sperr, G. Kögel and W. Triftshäuser, Nucl. Instr. and Meth. B **34**, 258 (1988).

[2] Willutzki, J. Störmer, G. Kögel, P. Sperr, D.T. Britton, R. Steindl and W. Triftshäuser, Meas. Sci. Technol. **5**, 548 (1994).

[3] C. G. Van de Walle and J. Neugebauer, j. Appl. Phys. **95**, 3851 (2004).

[4] S. Nakamura, M. Senoh, N. Iwasa, and T. Mukai, Jpn. J. Appl. Phys. **31**, 1258 (1992).

[5] J. Neugebauer and C. G. Van de Walle, Phys. Rev. Lett. **75**, 4452 (1995).

[6] J. Neugebauer and C. G. Van de Walle, Appl. Phys. Lett. **68**, 1829 (1996).

[7] H. Krause-Rehberg and H. S. Leipner, *Positron annihilation in semiconductors* (Springer-Verlag, Berlin, 1999).

[8] K. Saarinen, J. Nissilä, P. Hautojärvi, J. Likonen, T. Suski, I. Grzegory, B. Lucznik and S. Porowski, Appl. Phys. Lett. **75**, 2441 (1999).

[9] J. Oila, K. Saarinen, A. E. Wickenden, D. D. Koleske, R. L. Henry, and M. E. Twigg, Appl. Phys. Lett. **82**, 1021 (2003).

[10] K. Saarinen, T. Suski, I. Grzegory, and D. C. Look, Phys. Rev. B **64**, 233201 (2001).

[11] K. Saarinen, T. Laine, S. Kuisma, J. Nissilä, P. Hautojärvi, L. Dobrzynski, J. M. Baranowski, K. Pakula, R. Stepniewski, M. Wojdak, A. Wysmolek, T. Suski, M. Leszczynski, I. Grzegory, and S. Porowski, Phys. Rev. Lett. **79**, 3030 (1997).

[12] M. Alatalo, H. Kauppinen, K. Saarinen, M. J. Puska, J. Mäkinen, P. Hautojärvi, and R. M. Nieminen, Phys. Rev. B **51**, 4176 (1995).

[13] E. Calleja, M. A. Sánchez-García, D. Basak, F. J. Sánchez, F. Calle, P. Youinou, E. Muñoz, J. J. Serrano, J. M. Blanco, C. Villar, T. Laine, J. Oila, K. Saarinen, P. Hautojärvi, C. H. Molloy, D. J. Somerford, and I. Harrison, Phys. Rev. B **58**, 1550 (1998).

[14] M. Alatalo, B. Barbiellini, M. Hakala, H. Kauppinen, T. Korhonen, M. J. Puska, K. Saarinen, P. Hautojärvi, and R. M. Nieminen, Phys. Rev. B **54**, 2397 (1996).

[15] J. Neugebauer and C. G. Van de Walle, Phys. Rev. B **50**, 8067 (1994).

[16] F. A. Reboredo and S. T. Pantelides, Phys. Rev. Lett. **82**, 1887 (1999).

[17] A. F. Wright and T. R. Mattsson, J. Appl. Phys. **96**, 2015 (2004).

[18] E. R. Glaser, W. E. Carlos, G. C. B. Braga, J. A. Freitas, Jr., W. J. Moore, B. V. Shanabrook, R. L. Henry, A. E. Wickenden, D. D. Koleske, H. Obloh, P. Kozodoy, S. P. DenBaars, and U. K. Mishra, Phys. Rev. B **65**, 085312 (2002).

[19] K. Saarinen, P. Seppälä, J. Oila, P. Hautojärvi, C. Corbel, O. Briot and R. L. Aulombard, Appl. Phys. Lett. **73**, 3253 (1998).

[20] R. M. Nieminen, J. Laakkonen, P. Hautojärvi, and A. Vehanen, Phys. Rev. B **19**, 1397 (1979).

[21] T. E. M. Staab, M. Haugk, T. Frauenheim and H. S. Leipner, Phys. Rev. Lett. **83**, 5519 (1999).

[22] M. J. Puska and R. M. Nieminen, J. Phys. F **13**, 333 (1983).

[23] M. J. Puska and R. M. Nieminen, Rev. Mod. Phys. **66**, No. 3, (1994).

[24] E. Boronski and R. M. Nieminen, Phys. Rev. B **34**, 3820 (1986).

[25] W. Brandt and J. Reinheimer, Phys. Lett. A **35**, 109 (1971).

[26] R. Krause-Rehberg, H. S. Leipner, A. Kupsch, A. Polity, and Th. Drost, Phys. Rev. B **49**, 2385 (1994).

[27] R. Krause-Rehberg, M. Brohl, H. S. Leipner, Th. Drost, A. Polity, U. Beyer, and H. Alexander, Phys Rev. B **47**, 13266 (1993).

[28] J. Oila, V. Ranki, J. Kivioja, K. Saarinen, P. Hautojärvi, J. Likonen, J. M. Baranowski, K. Pakula, T. Suski, M. Leszczynski, and I. Grzegory , Phys. Rev. B **63**, 045205 (2001).

[29] K. Saarinen, P. Hautojärvi and C. Corbel, *Identification of Defects in Semi-conductors* (Academic, New York, 1998).

[30] M. J. Puska, C. Corbel and R. M. Nieminen, Phys. Rev. B **41**, 9980 (1990).

[31] J. Oila, J. Kivioja, V. Ranki, K. Saarinen, D. C. Look, R. J. Molnar, S. S. Park, S. K. Lee and J. Y Han, Appl. Phys. Lett. **82**, 3433 (2003).

[32] T. Mattila and R. M. Nieminen, Phys. Rev. B **55**, 9571 (1997).

[33] A. F. Wright, J. Appl. Phys. **90**, 1164 (2001).

[34] C. G. Van de Walle, Phys. Rev. B **56**, R10020 (1997).

[35] J. Neugebauer, and C. G. Van de Walle, Appl. Phys. Lett. **68**, 503 (1996).

[36] R. Niebuhr, K. Bachem, K. Dombrowski, M. Maier, W. Pletschen and U. Kaufmann, J. Electron. Mater **24**, 1531 (1995).

[37] A. Ishibashi, H. Takeishi, M. Mannoh, Y. Yabuuchi and Y. Ban, J. Electron. Mater. **25**, 799 (1996).

[38] S. O. Kucheyev, M. Toth, M. R. Phillips, J. S. Williams, C. Jagadish and G. Li, J. Appl. Phys. **91**, 5867 (2002).

[39] C. H. Scager, A. F. Wright, J. Yu and W. Götz, J. Appl. Phys. **92**, 6553 (2002).

[40] R. Armitage, Q. Yang, H. Feick, Y. Park and E. R. Weber, Mater. Res. Soc. Symp. Proc. **719**, F1.2 (2002).

[41] H. Tang, J. B. Webb, J. A. Bardwell, S. Raymond, J. Salzman and C. Uzan-Saguy, Appl. Phys. Lett. **78**, 757 (2001).

[42] A. Y. Polyakov, M. Shin, J. A. Freitas, M. Skowronski, D. W. Greve and R. G. Wilson, J. Appl. Phys. **80**, 6349 (1996).

[43] D. Kapolnek, S. Keller, R. Vetury, R. D. Underwood, P. Kozodoy, S. P. Den Baars and U. K. Mishra, Appl. Phys. Lett. **71**, 1204 (1997).

[44] D. B. Thomson, T. Gehrke, K. J. Linthicum, P. Rapagopal and R. F. Davis, MRS. Internet J. Nitride Semicond. Res. **4S1**, G3.37 (1999).

[45] Tsvetanka S. Zhaleva, Waeil M. Ashmawi, Ok-Hyun Nam, and Robert F. Davis, Appl. Phys. Lett **74**, 2492 (1999).

[46] F. Bertram, T. Riemann, J. Christen, A. Kaschner, A. Hoffmann,C. Thomsen, K. Hiramatsu, T. Shibata and N Sawaki, Appl. Phys. Lett. **74**, 359 (1999).

[47] S. Nitta, T. Kashima, M. Kariya, Y. Yukawa, S. Yamaguchi, H. Amano and I. Akasaki, MRS. J. Nitride Semicond. Res. **5S1**, W2.8 (2000).

[48] S. Nitta, T. Kashima, M. Kariya, S. Yamaguchi, H. Amano and I. Akasaki, Appl. Surf. Sci. **159-160**, 421 (2000).

[49] T. Paskova, E. Valcheva, J. Birch, S. Tungasmita, P.-O. Å. Persson, P. P. Paskov, S. Evtimova, M. Abrashev and B. Monemar, J. Crystal Growth **230**, 381 (2001).

[50] M. Rummukainen, J. Oila, A. Laakso, K. Saarinen, A. J. Ptak and T. H. Myers, Appl. Phys. Lett. **84**, 4887 (2004).